Available online at www.eccomasproceedia.org
Eccomas Proceedia SMART (2023) 1681-1690

ECCOMAS
Proceedia

X ECCOMAS Thematic Conference on Smart Structures and Materials
SMART 2023
D.A. Saravanos, A. Benjeddou, N. Chrysochoidis and T. Theodosiou (Eds)

SMART MACHINE ELEMENTS – SENSOR-INTEGRATED ELASTOMER COUPLINGS

Arthur Ewert[1], Johannes D. M. Menning[2], Artem Prokopchuk[3], Thomas Rosenlöcher[1], E.- F. Markus Henke[3], Thomas Wallmersperger[2], and Berthold Schlecht[1]

[1] Institute of Machine Elements and Machine Design, Technische Universität Dresden, Münchner Platz 3, 01069 Dresden
e-mail: arthur.ewert@tu-dresden.de

[2] Institute of Solid Mechanics, Technische Universität Dresden, George-Bähr-Str. 3c, 01069 Dresden

[3] Institute for Semiconductors and Microsystems, Technische Universität Dresden, Nöthnitzer Straße 64, 01069 Dresden

Abstract. The available computational performance is steadily increasing. On this basis, digital twins become possible, but the need for data increases. In mechanical engineering, research in recent decades has focused on providing data based on external sensors, e.g. accelerometers. In contrast, in recent years, effort have been made to provide data directly from a machine element itself. The aim of this work is to outline the concept of a sensor integrated machine element (SiME), using the example of a sensor-integrated jaw coupling for “in situ” data acquisition and transmission. Elastic couplings are an integral component of the drive train and hold vast development potential. The jaw coupling will be able to measure the transferred torque. The determination of the torque is based on the measurement of capacity changes resulting from the deformation of the elastic teeth of the gear rim. Based on the high deformations of the tooth, a soft strain sensor made of dielectric elastomer material (DES) is integrated. Furthermore, it can be shown that the rotational speed and shaft misalignments can be evaluated based on the same data. In order to evaluate the sensor-integrated coupling both a static and a dynamic test bench are described. Therefore, different load cases are defined to evaluate the performance of the jaw coupling. They are focused on the visco-elastic behaviour of the materials used for the elastic gear rim.

Key words: sensor-integration, jaw coupling, DES, elastic coupling, SiME

Peer-review under responsibility of the organizing committee of SMART 2023.
doi: 10.7712/150123.9939.444198

1 INTRODUCTION

Elastomer couplings are widely used machine elements that transmit power between two shafts while compensating for misalignment and shock loads. There is a variety of different designs that can be distinguished based on the main load condition that the elastomer experiences eg. compressive stress, bending stress and torsional shear stress. [1, 2] The focus of this paper will be couplings with compressed elastomer elements exemplified by the elastic jaw coupling as shown in Figure 1. The structure of the coupling typically consist of three main elements (i) two hubs and (ii) an elastomeric gear rim. The hubs have 2-5 cylindrical curved claws that interlock with the elastomeric gear rim. Depending on the size of the rim, it contains 4-10 rounded teeth. The gear rim is typical made of thermoplastic polyurethane (TPU) with various hardnesses. As torque is transmitted from on hub to the other, the teeth are deformed, compensating for radial, angular and axial misalignment's as well as absorb shocks from the drive system.

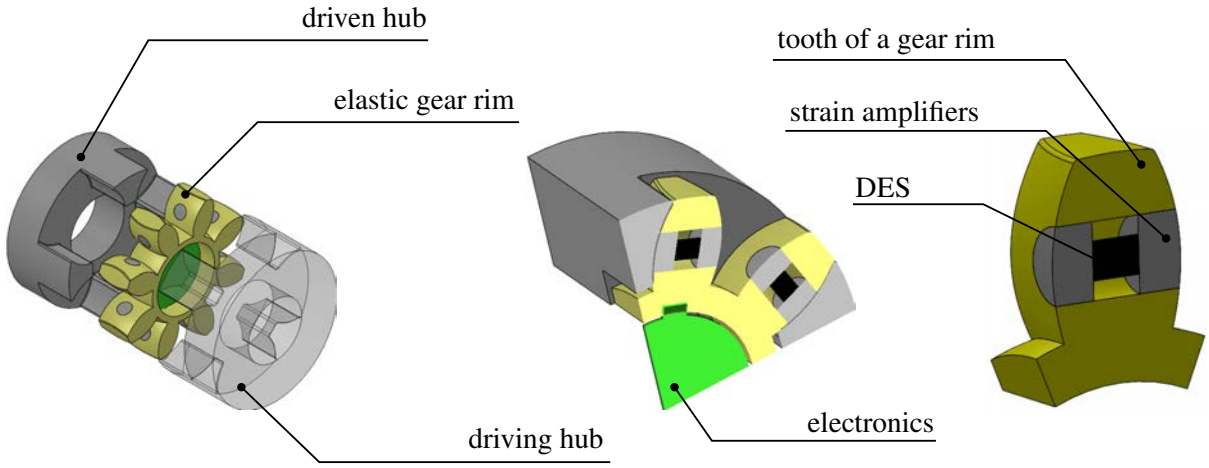

Figure 1: Concept of a elastic jaw coupling with an integrated dielectric elastomer sensor in the teeth of the gear rim.

The sensor-integration into the mechanical element (SiME) would enable the coupling to ïn situm̈easure the transmitted torque between two shafts and their misalignment's. This holds a vast development potential, in particular for the acquisition of relevant system and process variables in the drive train such as transmitted torque, rotational speed, temperature or shaft misalignment. The aim of the current work is to outlay the concept of a sensor-integrated jaw coupling (SiME) and to investigate the influences of shaft misalignment on the measurement signal of the SiME.
Therefore the measurement chain and the sensor integration are described in section 2. Furthermore two test benches for the evaluation of the SiME are described in section 4 including experimental load cases in section 4.1 and 4.2. Shaft misalignment can increase the loads for the coupling and shafts and are a common failure mode for couplings as shown by [3], but to the

knowledge of the authors there is no literature for the resulting loads on the teeth of the gear rim for elastic jaw couplings. In order to interpret the measurement signals correctly a multibody-system simulation model (MBS) is developed. Using this model the transmitted force by a tooth during an rotation is evaluated based on radial and angular displacement in section 5.

2 SENSOR INTEGRATION

The sensor-integration would enable the coupling to "in situ" measure the transmitted torque between two shafts and their misalignment. Previously this was only possible if spacious and expensive measurement equipment was used, mainly focusing on application of strain gauge on shafts or the use of accelerometers. [1] Schork et al. have proposed a SiME jaw coupling in [4]. They have equipped one tooth of the gear rim with a strain gauge, disabling the tooth's ability to transmit forces significantly. Based on the high deformation of the teeth conventional sensors like strain gauges are not applicable, if the tooth should still be able to carry loads. Therefore soft strain sensors namely dielectric elastomer sensors (DES) are applied, as they are able to withstand the deformations in the coupling. The concept of the DES, their manufacturing process and more details are further explained in Prokopchuk et al. [5]. For the sensor-integration process one DES is placed in a central borehole of every teeth in the gear rim. This placement causes the DES to deform if the surrounding material of the teeth is deformed. DES behave electrically like plate capacitors [6]. The highly deformable plate capacitor is oriented so that the normal direction of the capacitor plates are perpendicular to the effective direction of the transmitted force by a tooth. The sensor-integrated jaw coupling is displayed in Figure 1. If torque is applied, the teeth are deformed, resulting in a deformation of the DES. If the DES is deformed the internal capacitors are deformed too and therefor the distance h_{plates} between the capacitor plates decreases, leading to an increase of capacity, since the capacity is proportional to the inverse of the plate distance $C \propto 1/h_{\mathrm{plates}}$. Hence resulting in a measurable change of capacity that is determined by the applied load. In order to increase the sensitivity of the sensor, mechanical amplifiers are used. This strain amplifier increases the relative deformation of the DES due to its significantly higher stiffness. Additionally the amplifier serves as a protective border between DES and the claws of the hubs. Furthermore, the temperature is measured, since the non-linear stiffness of the TPU is highly temperature-dependent and decreases with increasing temperature [7].

3 METHODS

The aim of this work is to determine the applied load on a tooth during a rotation while misalignments are applied to the coupling. It is necessary to consider the forces for possible operating points during deployment of the SiME, which are determined by (i) the radial displacement K_{r}, (ii) the angular displacement K_{w}, and (iii) the angle between the displacements ζ, leading to a three dimensional parameter field. The transmitted torque is not considered here, because it scales directly with the applied load on a tooth. The definitions for the misalignments K_{r}, K_{w} and ζ are shown in Figure 2a. The driven hub is considered to be fixed but rotatable.

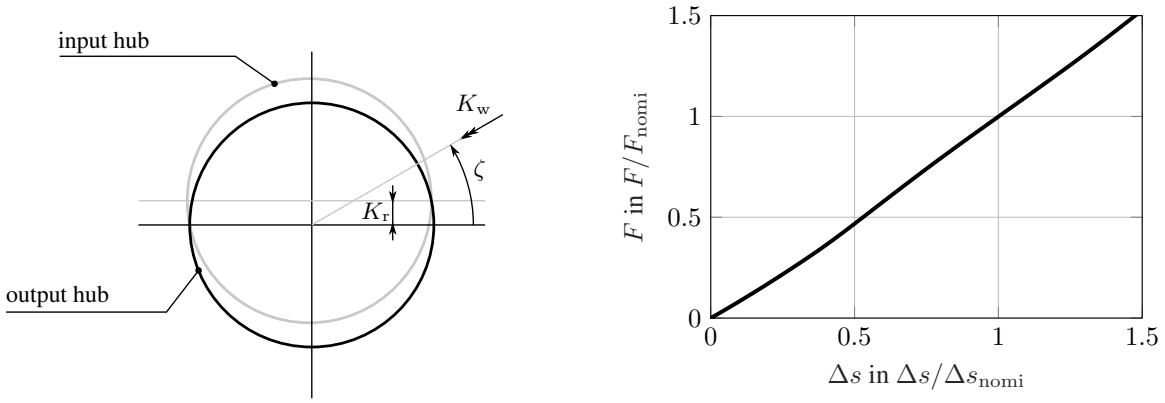

(a) Definition of the misalignments K_r, K_w and ζ of the coupling

(b) Force-displacement characteristic derived from the torsion-torque characteristic by [7]

Figure 2: Definition of the applied shaft misalignment's and the characteristic displacement-force characteristic used for the parameterization.

The driving hub is rotatable too and can be additionally displaced as shown in Figure 2a. The displacements are defined as follows: the radial displacement is defined as the radial distance between the rotational axis of the hubs in the plane view of the coupling. The angular displacement is defined as the intersection angle of the rotational-axis of the hubs. ζ is defined as the angle between the direction of radial displacement and the resulting rotation perpendicular to the main rotary axis of the driving hub.

In order to determine the applied load on a tooth it is necessary to know the torsion-torque characteristic of the coupling. Few sources are available regarding this subject, Sladkowski and Opasiak [8], Bilgar et al. [9], and Menning et al. [7] modelled an elastomeric jaw coupling. Only Menning et al. have developed a detailed finite element model for the calculation of the coupling, but the calculation times for the model are very high, due to the visco-elasticity of the material and the changing contact areas during loading. Considering the parameter field a faster method is necessary. Therefore a multibody-system simulation (MBS) model using SimPack is applied. The elastic gear rim is reduced to eight Force-Elements, each representing a tooth of the rim, which interlock with the hubs. Their stiffness is modelled based on the static torsion-torque characteristic derived from the finite element model by Menning et al. [7] and considered through a lookup table in the force element. This characteristic is shown in Figure 2b. The Force F and the displacement Δs are normalised by using the nominal operation point (F_nomi & Δs_nomi) for $\vartheta = 23\,^\circ\mathrm{C}$. Thermal dependency's are not included and the temperature for the torsion-torque characteristic is chosen as $\vartheta = 23\,^\circ\mathrm{C}$. The force elements are configured so that exclusively compression forces act on them. To simplify the analysis, damping has been neglected here. During loading the driving hub applies a torque up to the nominal torque T_nomi, while the driven hub applies an equal inverted torque, resulting in tensioning of the coupling. Additional the driving hub can translate and tilt. Using this model the parameter field for K_r,

K_{w}, and ζ, with respectively $n_{\mathrm{op}} = 10$ operating points per free variable, can be calculated quickly.

4 EXPERIMENTAL DESIGN

In the following section two experimental test benches are described: (i) a static test-bench which focuses on the determination of the characteristics parameters of the coupling and fast iteration of the DES designs, and (ii) a dynamic test-bench which focuses on the performance evaluation of the entire sensor system under real load conditions.

4.1 Static test-bench

The concept of the test bench is displayed in Figure 3. The specimen (3) is placed in between two bellow couplings (2) with a torsional stiffness of $c_{\mathrm{t}} = 780\,\mathrm{kNm/rad}$. The stiffness of the bellow coupling is chosen to be significantly greater then that of the specimen being tested. A hydraulic pivot motor (1) applies the torque to the load line. The driven hub of the specimen is fixed and the driving hub follows the applied twisting of the pivot motor. Torque and displacement are measured, additionally the temperature off the specimen can easily be measured.
Based on this design (i) specimens can be quickly changed, (ii) various characteristic load conditions can be applied. And (iii) the sensor-integrated coupling can be contacted using wires without the need for transmission electronics or the sensor can be directly connected to laboratory measurement equipment, since the specimen is not rotating. Furthermore operation conditions e.g. frequencies and loads can be quickly adapted due to the pivot motor.

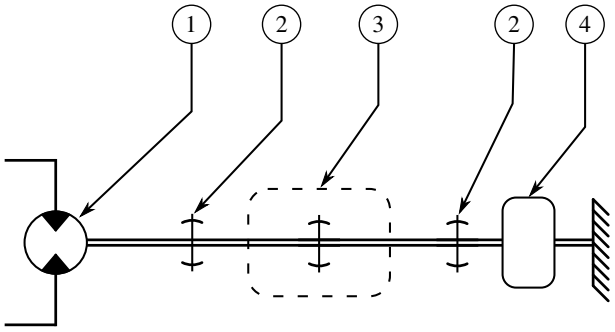

Figure 3: Concept of a static test bench for an elastomeric jaw coupling.

Using this approach the frequencies for loading are limited to about $f = 20\,\mathrm{Hz}$ by the pivot motor and the valve, depending on the used deformation amplitudes. In addition, the application of misalignment is not possible in this design because the loaded teeth always experience the same loads. For testing five instructions have been developed: (i) sinusoidal loading with loading speeds identical to the rate dependent test for parameter identification of the TPU material, (ii) incremental stress relaxation test, (iii) continuous high frequency sinusoidal loading, for heating and dissipation measurements, (iv) frequency sweep with constant amplitude and octave wise frequency increase, and (v) static loading, for torque torsion characteristic.

4.2 Dynamic test-bench

In order to test the coupling under realistic load conditions with realistic speeds a dynamic test bench is proposed cf. Figure 4. The test bench is made of two interconnected gear boxes (4) which are tensed by the tensioning-coupling (3) resulting in a circulating torque which is commonly used [10, 11] technique. Using this approach only the power loss needs to be provided by the drive unit (5). On the driving side the specimen (1) is connected to a movable cross table (2) which can dynamical translate and tilt and therefore apply displacements in K_r and K_w direction. Based on this design (i) the specimens can be tested under realistic use cases with the appropriate rotational speeds, and (ii) shaft misalignments are realisable, which can be dynamically set even under load conditions. It follows that using this test bench the SiME can undergo a full system prove of concept. On the other side the setup times for testing a specimen are high and they are difficult to access. Furthermore maintenance and peripheral components including lubrication holds additional challenges.

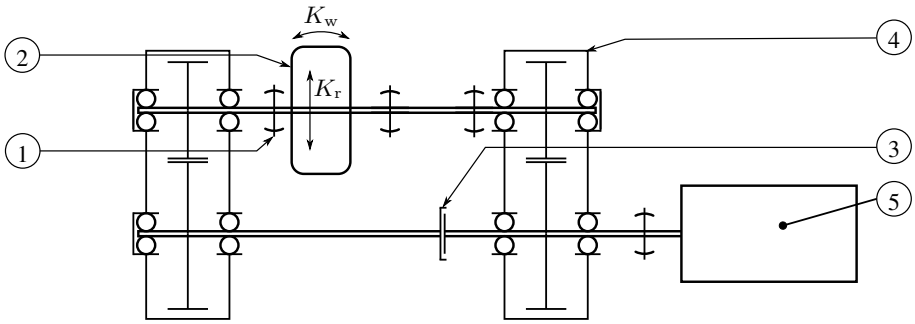

Figure 4: Concept of a dynamic test bench for an elastomeric jaw coupling with adjustable radial and angular displacement for the coupling.

5 RESULTS

The basic radial force in a tooth during loading of the coupling is displayed in Figure 5. In the first section from $t = 0\,\mathrm{sec} \ldots 1\,\mathrm{sec}$ the coupling is loaded until the nominal torque $T = T_\mathrm{nomi}$ is reached. After loading, the rotation of the coupling is initiated with a rotational speed of $n = 60\,\mathrm{rpm}$. It is evident, that the tooth force is constant during a rotation, if no displacements are applied to the shaft hubs. This force will be herein after referred to the nominal force F_nomi. Furthermore only half of the teeth, in this case all odd numbers of teeth, are transmitting loads, while teeth with even numbers transmit no loads. This load distribution is typical for jaw couplings and based on their geometry.

If a displacement is applied the characteristic behaviour, as shown in Figure 5, can be observed. Here the transmitted force is oscillation around the nominal force F_nomi with a characteristic amplitude $\hat{F}$ and frequency Ω. The frequency is equal to the rotational speed n. The sinusoidal behaviour of the force for each teeth is additionally shifted by φ in $\varphi = n_\mathrm{teeth}/4 \cdot \pi$ increments. Therefore the characteristic can be described using

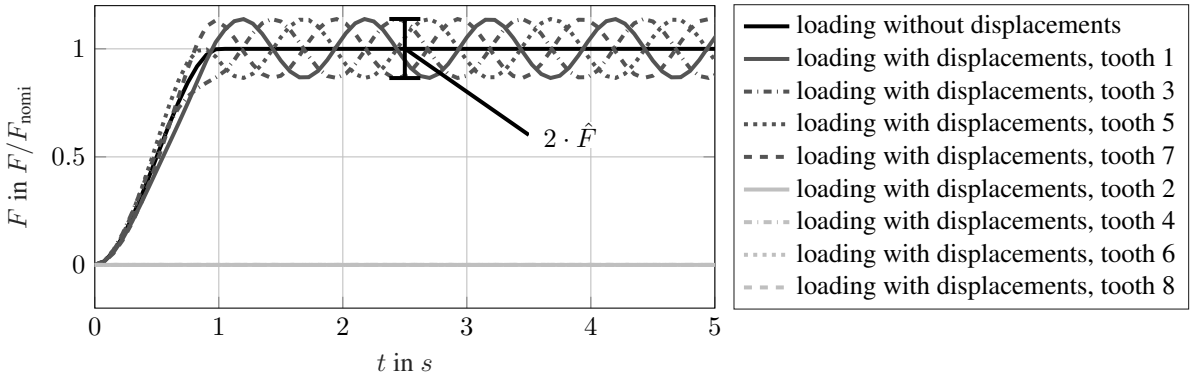

Figure 5: Transmitted force of a tooth over time during loading up to $T = T_{\mathrm{nomi}}$ and the general characteristic of the transmitted force with applied misalignments, exemplified by a displacement of $K_{\mathrm{r}}/K_{\mathrm{r,max}} = 0.89$ and $K_{\mathrm{w}}/K_{\mathrm{w,max}} = 0.11$.

$$F = F_{\mathrm{nomi}} \cdot \left(1 + \hat{F} \cdot \sin\left(\Omega + n_{\mathrm{teeth}}/4 \cdot \pi\right)\right). \tag{1}$$

In order to evaluate the influence of one misalignment on the amplitude $\hat{F}$ Figure 6a can be used. It is evident that a radial displacement K_{r} has a higher influence with up to $\hat{F} = 0.151$ compared to an angular displacement K_{w} with an amplitude of $\hat{F} = 0.043$.

Since under real operation condition both displacements are commonly present, the parameter field for K_{r} and K_{r} is of interest. This field is displayed in Figure 6b. Here the angle ζ between K_{r} and K_{r} is set to $\zeta = 0\,\mathrm{deg}$. Based on the results it is evident that in the case of $\zeta = 0\,\mathrm{deg}$ the amplitudes are not simply addable but rather almost cancel each other if K_{r} is in the range of $K_{\mathrm{r}} = 0 \ldots 0.4$. Furthermore an additional angular displacement K_{w} reduces the amplitude $\hat{F}$ if the radial displacement is high.

As described above the radial and angular misalignments can have a significant impact on the force in a tooth during a rotation of the coupling. To further investigate this, the influence of ζ with a varying radial displacement K_{r} and a constant angular displacement of $K_{\mathrm{w}}/K_{\mathrm{w,max}} = 1$ is analysed. The Figure 6c presents a polar plot of the force amplitude $\hat{F}$ in radial direction, against the angle ζ, highlighting the influence of ζ. A darker line colour indicates a higher radial displacement $K_{\mathrm{r}}/K_{\mathrm{r,max}}$. It is evident that the amplitudes $\hat{F}$ reach a minimum if ζ is $\zeta = 0\,\mathrm{deg}$ and reach a maximum at an angle of $\zeta = 180\,\mathrm{deg}$. Furthermore the displacements cancel each other out at $\zeta = 0\,\mathrm{deg}$ with a radial displacement K_{r} of $K_{\mathrm{r}}/K_{\mathrm{r,max}} = 0.33$. Comparing this result with the data from Figure 6a, it is evident that the amplitudes $\hat{F}$ from K_{r} and K_{w} must be phase shifted by $\varphi = 180\,\mathrm{deg}$ in order to cancel each other out. This is confirmed by the fact, that the maximum $\hat{F}$ is at the opposite side at $\zeta = 180\,\mathrm{deg}$, and reaches an amplitude of $\hat{F} \approx 0.2$, which is the sum of the amplitudes from radial and angular displacement. Using

$$\hat{F} = \left|\hat{F}_{\mathrm{r}}\left(K_{\mathrm{r}}\right) \cdot e^{\mathrm{i}2\pi} + \hat{F}_{\mathrm{w}}\left(K_{\mathrm{w}}\right) \cdot e^{\mathrm{i}(\zeta+\pi)}\right|, \tag{2}$$

the resulting force amplitude $\hat{F}$ in a tooth can be determined by the amplitudes $\hat{F}_\mathrm{r}$ and $\hat{F}_\mathrm{w}$ inferable by K_r and K_w and the angle between the displacements ζ.

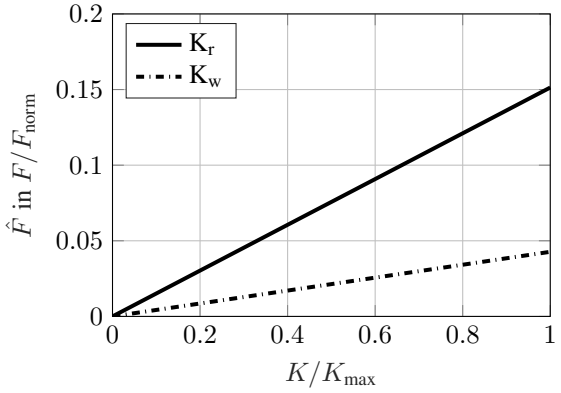

(a) Influence of radial and angular misalignments on the characteristic force amplitude $\hat{F}$

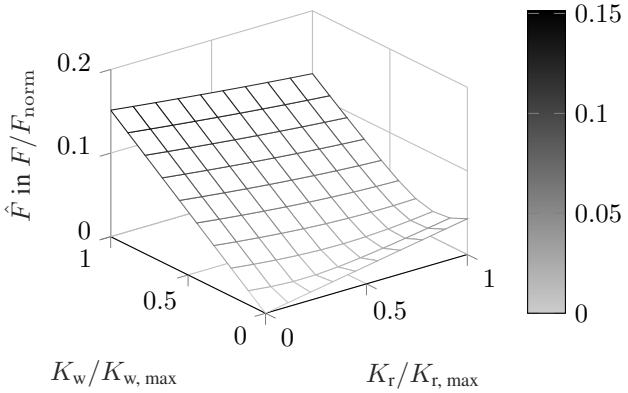

(b) Parameter field for misalignments on the characteristic force amplitude $\hat{F}$ at $\zeta = 45\,\mathrm{deg}$

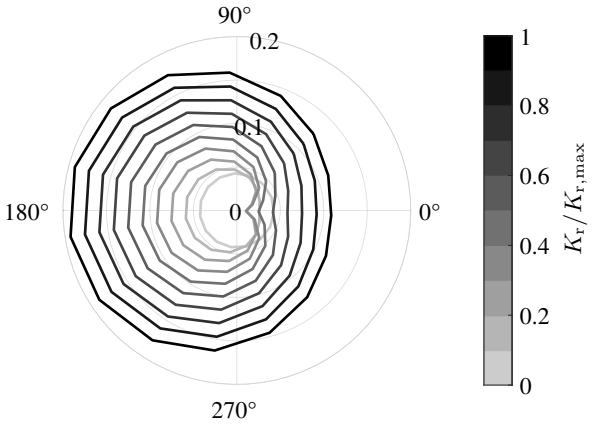

(c) Results of varying radial misalignment with constant angular displacement of $K_\mathrm{w}/K_\mathrm{w,max} = 1$ on the characteristic force amplitude $\hat{F}$ with a varying angle between the displacements ζ.

Figure 6: Influence of radial, angular misalignments K_r, K_w and the angle between those ζ on the characteristic force amplitude $\hat{F}$.

6 CONCLUSIONS

In this paper the basic concept of a sensor-integrated elastomeric jaw coupling for an ”in situ” measurement of the transmitted torque is outlined. Both a static and a dynamic test-bench are described. They can be used for in depth experimental examinations of the behaviour of the coupling and the sensor-integrated coupling. They serve as a test bench for the validation of numerical models and for a successively or fully integrated test of a sensor-integrate coupling.

The couplings are generally used to compensate for misalignments the influence of these misalignments, namely radial displacement K_{r}, angular displacement K_{w} and the angle between these displacements ζ is investigated. This is of importance, since based on the integration concept the force transmitted by a tooth is measured. Using a MBS-model, parameterised based on a finite element model from Menning et al. [7] for elastic jaw couplings, it was shown that the displacements induct a sinusoidal fluctuation of the transmitted force. The amplitude $\hat{F}$ can reach, depending on the amount of displacement and the specific angle, up to $\hat{F} = 20\,\%$ of the nominal force F_{nomi} when compared to aligned shaft hubs. Furthermore it was shown that angular and radial displacement will be difficult to distinguish in a measured signal because both displacements result in a sinusoidal load with the same frequency, which is directly proportional to the rotational speed of the coupling. The next step will be the construction of a prototype of the sensor-integrated coupling and its validation using the proposed test benches.

Acknowledgement The support of the German Science Foundation (DFG) within the grants WA 2323/21-1, HE 7385/3-1, SCHL 1736/8-1 (project number: 441853410 and 466661922) is gratefully acknowledged.

REFERENCES

[1] B. Schlecht, *Maschinenelemente 1 Festigkeit, Wellen, Verbindungen, Federn, Kupplungen*, 2nd ed. Pearson Studium, 2015.

[2] H. Peeken and C. Troeder, *Elastische Kupplungen Ausführungen, Eigenschaften, Berechnungen*. Berlin: Springer, 1986.

[3] L. Barik, S. Samal, A. Behera, D. K. Rajak, and C. I. Pruncu, "On the replacement of steel by nitinol as coupling agent in automobile shaft," *ISSS Journal of Micro and Smart Systems*, vol. 10, no. 2, pp. 87–102, 2021.

[4] S. Schork, S. Gramlich, and E. Kirchner, "Entwicklung von Smart Machine Elements – Ansatz einer smarten Ausgleichskupplung," *Design for X*, vol. 27, pp. 181–192, 2016.

[5] A. Prokopchuk, A. Ewert, J. Menning, A. Richter, B. Schlecht, T. Wallmersperger, and E.-F. M. Henke, "Manufacturing of soft capacitive strain sensor based on dielectric elastomeric material for an elastic element of a jaw coupling," *submitted to Smart Materials and Structures*, 2023.

[6] M. Franke, A. Ehrenhofer, S. Lahiri, E.-F. Henke, T. Wallmersperger, and A. Richter, "Dielectric elastomer actuator driven soft robotic structures with bioinspired skeletal and muscular reinforcement," *Frontiers in Robotics and AI*, vol. 7, p. 510757, 2020.

[7] J. Menning, A. Ewert, A. Prokopchuk, B. Schlecht, M. Henke, and T. Wallmersperger, "Finite element based modeling and simulation of an elastomer gear rim," *accepted in PAMM*, 2023.

[8] A. Sładkowski and T. Opasiak, "FEM model of flexible coupling ASR type," *Transport Problems*, vol. 2, no. 3, pp. 109–114, 2007.

[9] M. Y. Biglar, G. Payganeh, and A. Shirafkan, "Calculation of elastic deformation error of thermoplastic polyurethane flexible couplings in computer numerical control devices," *Proceedings of the Institution of Mechanical Engineers, Part B: Journal of Engineering Manufacture*, vol. 230, no. 9, pp. 1684–1689, 2016.

[10] DIN 3990-16:2020-05, "Tragfähigkeitsberechnung von Stirnrädern - Teil 16: Bestimmung der Graufleckentragfähigkeit von Schmierstoffen im FZG-Prüfverfahren GT-C/8,3/90," Berlin, 2020.

[11] C. Bauer, "Untersuchung der Tragfähigkeit von Verzahnungen bezüglich zahninternen Versagens," Ph.D. dissertation, TU Dresden, 11 2017.